Solitons in the paramagnetic and partially disordered phases of $CsCoCl_3$

J. P. Boucher*
Département de Recherche Fondamentale, Section de Résonance Magnétique, Centre d'Etudes Nucléaires de Grenoble, F-38041 Grenoble Cedex, France

L. P. Regnault and J. Rossat-Mignod
Département de Recherche Fondamentale, Laboratoire de Diffraction Neutronique, Centre d'Etudes Nucléaires de Grenoble, F-38041 Grenoble Cedex, France

Y. Henry
Laboratoire d'Electronique et de Technologie de l'Information, Laboratoire de Cristallogéuèse et Recherche sur les Matériaux, Centre d'Etudes Nucléaires de Grenoble, F-38041 Grenoble Cedex, France

J. Bouillot and W. G. Stirling
Institut Laue-Langevin, F-38042 Grenoble Cedex, France
(Received 29 May 1984)

We present a detailed quantitative experimental analysis of the soliton regime in a one-dimensional (1D) quantum spin system. The experiments were performed on the 1D antiferromagnet $CsCoCl_3$. As well as soliton fluctuations, a 1D antiferromagnetic mode was observed in both the paramagnetic ($T > T_{N1} \simeq 21$ K) and the partially disordered ($T < T_{N1}$) phases. This result proves that, below T_{N1}, one third of the chains remains in a paramagnetic state with fluctuations governed by solitons. In a semiphenomenological model the collisions between solitons are explicitly taken into account in our description, yielding good agreement between theory and experiment over the whole temperature range.

I. INTRODUCTION

In recent years, a great deal of work has been devoted to the study of nonlinear excitations in one-dimensional (1D) magnetic systems. Planar antiferromagnetic (AF) chains with classical spins ($S \gg 1$) have been shown to provide a good model for solitons,[1] where they can be viewed as Bloch walls extending over several lattice units (10 to 30). In such a case of "broad" solitons, the comparison between theory and experiment is remarkably good. For Ising AF chains ($S = \frac{1}{2}$), a soliton model has also been proposed by Villain.[2] In this case, the walls are reduced to one lattice unit. Such "narrow" solitons should exhibit propagating behavior. The compound $CsCoCl_3$ is known to be a good realization of Ising AF chains. Characteristic fluctuations centered at zero frequency have previously been observed which agree with the soliton picture.[3] However, strong discrepancies remain with the predictions of Villain's model, which, indeed, is restricted to the case of noninteracting solitons. Recently, the compound $CsCoBr_3$ has been shown to be also a good candidate for studying narrow solitons.[4] In the compound to be studied here, $CsCoCl_3$, the 1D short-range-order regime where the picture of moving solitons is meaningful extends from $T \simeq 75$ K—this value corresponds to the maximum of the susceptibility in the paramagnetic phase[5]—down to the Néel temperature $T_{N1} \simeq 21$ K.[6] At this temperature and below, long-range order exists between chains. The magnetically ordered phases in $CsCoBr_3$ and $CsCoCl_3$ have been widely investigated.[6] In the c plane perpendicular to the chains the spins form a triangular lattice which could promote frustration effects. It is argued that at $T < T_{N1}$, since the 1D short-range order is already well developed, the magnetic chains as a whole should behave like a single moment. Then, with an AF coupling between chains, one can be led to the simplest situation for frustration: One third of these "single" moments should remain "disordered." The magnetic structure observed below T_{N1} in $CsCoCl_3$ (Ref. 6) agrees with this model which implies that one third of the chains be maintained in a paramagnetic state. In other words, 1D soliton fluctuations should be observable even below T_{N1}. Experimentally, only one result seems to agree with this description. This is the electron paramagnetic resonance observed by Adachi[7] *below* T_{N1} down to a few degrees Kelvin.

In the present paper, we report an exhaustive neutron investigation performed on the compound $CsCoCl_3$. Both wave vector q and frequency ω analyses could be made with very high instrumental resolution. Low-frequency fluctuations associated directly with the soliton excitations as well as those associated with short range order have been investigated. The data are compared with a soliton model which takes into account explicitly the collisions between solitons. The experimental study was performed over a wide temperature range, in both the paramagnetic and partially disordered (PD) phases, above and below T_{N1}, respectively.

II. SOLITON FLUCTUATIONS

In this section, we briefly sketch the theoretical description that we shall use for the interpretation of our experimental results. Assuming the chain axis to be along z, the 1D antiferromagnetic Hamiltonian for $CsCoCl_3$ can be written as

$$\mathcal{H}=\sum_n 2JS_n^zS_{n+1}^z+\epsilon J(S_n^+S_{n+1}^-+S_n^-S_{n+1}^+)\ , \qquad (2.1)$$

with $S=\frac{1}{2}$, $J=75$ K, and $\epsilon\simeq 0.12$.[3]

The thermodynamics being governed essentially by the first term of Eq. (2.1), the static two-spin correlation functions can be expressed in reciprocal space as[2]

$$\langle S_q^zS_{-q}^z\rangle=\frac{S^2}{2\pi}\frac{e^{\kappa}(1-e^{-2\kappa})}{e^{\kappa}(1-e^{-\kappa})^2+4\cos^2(q/2)}\ ,$$

with $e^{-\kappa}=\tanh(J/2T)$, where T is the temperature. For $T\ll J$, we get

$$\langle S_q^zS_{-q}^z\rangle\simeq\frac{S^2}{2\pi}\frac{2\kappa}{\kappa^2+4\cos^2(q/2)}$$

In these equations, the wave vector q is expressed in reduced units (the chain parameter $c=1$). As a consequence Γ_q is dimensionless and the inverse quantity Γ_q^{-1} evaluates directly the average number of correlated spins in a chain. In the following, these units for q and Γ_q are retained except in some cases describing the experimental values chosen for the scattering vectors Q which, as usual, are expressed in reciprocal lattice units (rlu). This static correlation function is centered at $q=\pi$. Its width (half-width at half maximum) Γ_q gives a measure of the inverse of the correlation length ξ;

$$\Gamma_q=\xi^{-1}\simeq\kappa\simeq 2e^{-J/T}\ . \qquad (2.2)$$

As shown by Villain,[2] the dynamics are described at low T by propagating elementary excitations associated with domain walls (solitons) separating the ordered domains of length ξ. The mobility of these solitons is ensured by the second terms of Eq. (2.1). The corresponding fluctuations are represented in Fig. 1. Depending on the wave vector q to be considered with respect to Γ_q, namely, $q^*=|\pi-q|\lesssim\Gamma_q$ or $q^*\gg\Gamma_q$, two different types of fluctuations can be observed.

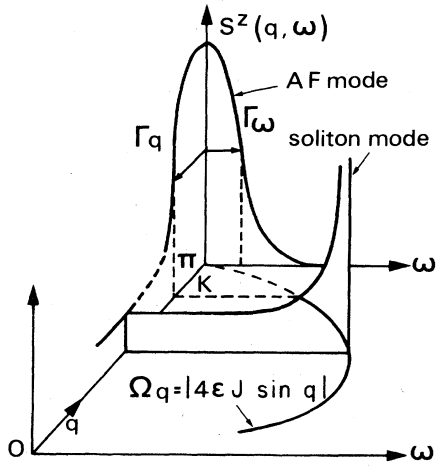

FIG. 1. Dynamical structure factor for the fluctuations parallel to the chain axis as predicted by the description of Villain (Ref. 2). Γ_q and Γ_ω are defined by Eqs. (2.2) and (2.4) and Ω_q by Eq. (2.12). κ is the inverse correlation length.

A. Antiferromagnetic (AF) mode ($q\simeq\pi$)

For $q^*\lesssim\Gamma_q$, the observed fluctuations concern essentially the ordered domains, which can then be considered as a whole. They give rise to the so-called (1D) AF mode centered at $q=\pi$ and $\omega=0$ (Fig. 1). In the soliton model, the width Γ_q which measures the short-range order is simply the soliton density n_s. One has

$$\Gamma_q=\xi^{-1}=2n_s$$

(the factor of 2 accounts for the two possible directions of the spins in the 1D magnetic sublattices). For $T\ll J$, we deduce from Eq. (2.2) the soliton density to be given by

$$n_s=e^{-J/T}\ . \qquad (2.3)$$

Concerning the dynamics, each time a soliton goes through an ordered domain a flipping is induced which makes the two AF sublattices exchange their spin orientation. The frequency broadening of the AF mode results from these flippings. The frequency width Γ_ω measures the corresponding flipping rate which for a "coherent" motion is given by

$$\Gamma_\omega=2n_sV_0=\Gamma_qV_0\ , \qquad (2.4)$$

where V_0 is the average velocity of the solitons. This quantity is derived explicitly in Appendix C [Eq. (C1)]:

$$V_0=\frac{2}{\pi}\frac{\sinh(2\epsilon J/T)}{2\epsilon J/T}\frac{4\epsilon J}{I_0(2\epsilon J/T)}\ , \qquad (2.5)$$

where $I_0(X)$ is the modified Bessel function. In the limits $2\epsilon J\ll T\ll J$, we get from (2.4)

$$\Gamma_\omega\simeq\frac{16}{\pi}\epsilon Je^{-J/T}\ . \qquad (2.6)$$

The shape of the AF mode is also a characteristic of the soliton mobility. Maki has suggested the following expression for the coherent model:[8]

$$S^z(q,\omega)=\frac{S^2}{2\pi}\frac{\Gamma_\omega^2/\Gamma_q}{\{\Gamma_\omega^2[1+(q^*)^2/\Gamma_q^2]+\omega^2\}^{3/2}}\ , \qquad (2.7)$$

which differs appreciably from the (simpler) Lorentzian form (see Appendix C). In particular the widths full width at half maximum (FWHM) are given by

$$\Delta_\omega=1.53\Gamma_\omega[1+(q^*)^2/\Gamma_q^2]^{1/2}\ ,$$
$$\Delta_q=1.53\Gamma_q(1+\omega^2/\Gamma_\omega^2)^{1/2}\ . \qquad (2.8)$$

Equation (2.7) is only a convenient approximation, but is certainly sufficient for analyzing our neutron data (a similar discussion is given in Ref. 9). However it is worth noting, as shown in Appendix C, that in the present case of narrow solitons, the lower the temperature is compared to $2\epsilon J$ ($T\ll 2\epsilon J$), the better is the approximation.

One purpose of the present work is to complete the investigation of the 1D AF mode.[3,10] In particular, it is essential to obtain quantitative information on Γ_ω to determine the soliton dynamics. At the Néel temperature, $T_{N1}\simeq 21$ K, the physical frequency width for example, can be evaluated from Eq. (2.8) to be only

$$\Gamma_\omega = 0.023 \text{ THz} \tag{2.9}$$

at $q^*=0$ $(q=\pi)$. The investigation of this AF mode, especially if it is extended to lower temperatures, $T<T_{N1}$, requires excellent instrumental resolution, in both wave vector and energy.

B. Soliton modes ($q^* = |\pi - q| \gg \Gamma_q$)

The fluctuations observed for $q^* \gg \Gamma_q$ are directly concerned with the propagation of the soliton excitations. The initial calculation presented by Villain[2] is basically performed in the subspace E_1 of states containing only one such elementary excitation. As a result the corresponding fluctuations are weighted by an exponential activation term, $\exp(-J/T)$—simply the soliton density [Eq. (2.3)]—since the energy needed to create one soliton is actually $E_1 \simeq J$. A similar but simplified derivation is presented in Appendix A. Recently another calculation has been made by considering the subspace E_2 of two elementary excitations.[11] The weighting term is therefore $\exp(-2J/T)$. However, the authors state that due to transitions within all the excited-state manifolds, their description should lead to the same result as the Villain evaluation.

In subspace E_1, the propagation of the solitons is ensured by elementary plane waves of vector k with the energy

$$\omega(k) = J + 2\epsilon J \cos(2k) . \tag{2.10}$$

As shown in Appendix A, the calculation of the soliton modes is performed entirely within E_1. At an intermediate stage we obtain for the spin component *parallel* to the chains, for instance, the following expression:

$$S^z(q,\omega) = \frac{S^2}{\pi^2} \frac{n_s}{4\cos^2(q/2)} \int_0^{2\pi} dl\, p\left[\frac{l+q}{2}\right] \times \delta[\Omega_q \sin(l) - \omega] , \tag{2.11}$$

where $p(k)$ is the distribution probability amongst the different elementary waves of E_1:

$$p(k) = e^{-2\epsilon J \cos(2k/T)} \Big/ \sum_k e^{-2\epsilon J \cos(2k/T)} ,$$

and where Ω_q defines the soliton dispersion frequency

$$\Omega_q = 4\epsilon J \,|\sin q| . \tag{2.12}$$

In Eq. (2.11) the energy conservation can be seen to be guaranteed for each component l of the space E_1 through the function $\delta(x)$.

A characteristic square-root divergency of the soliton mode arises immediately from Eq. (2.11) yielding the result of Villain,[2]

$$S^z(q,\omega) = \frac{S^2}{2\pi^2} \frac{2\kappa}{4\cos^2(q/2)} \frac{e^{\omega/(2T)}}{I_0(2\epsilon J/T)} \times \frac{\cosh\{\cot[q(\Omega_q^2-\omega^2)^{1/2}/(2T)]\}}{(\Omega_q^2-\omega^2)^{1/2}} .$$

A very similar relation is obtained for the transverse spin components [Eq. (A8)].

The square-root divergency at Ω_q is clearly unrealistic and one expects the collisions with solitons and/or with other excitations to "round off" the peak. As mentioned by Villain,[2] such a derivation is limited to short times *before* any collision takes place. We can try to evaluate the characteristic time τ_c associated with the collisions, or equivalently the collision rate $\omega^c = \tau_c^{-1}$.

First we note that the predominant collision process will be that between solitons. For instance, since the subspace E_2 with two elementary excitations, which includes also the spin waves (magnons), is defined at an energy level which is twice the energy of E_1, the number of magnons contributing to the collisions is comparatively small.

Second, extending a suggestion already outlined in Ref. 2, we consider the effects of collisions directly on each state k of E_1. The corresponding energy levels are expected to be broadened, the broadening is given by the collision rate. For a soliton in a state k, we write it as

$$\Delta^c(k) \simeq n_s \sum_{\substack{k'=-\pi \\ (k'\neq k)}}^{+\pi} p(k') \,|V_{k'} - V_k| , \tag{2.13}$$

where the soliton velocity V_k is defined from Eq. (2.10)

$$V_k = \frac{d\omega(k)}{dk} = -4\epsilon J \sin(2k) .$$

Before going further, it might be worth comparing this procedure to the result obtained by Allroth and Mikeska for the case of collisions between classical solitons and magnons in planar ferromagnetic chains.[12] Any magnon mode is expected to be broadened by the collisions with the solitons. For a given magnon propagating with the wave vector q the corresponding width is given by the collision rate defined by

$$\omega_q^c \simeq n_s \left[V_0 + \frac{d\omega_q}{dq}\right] , \tag{2.14}$$

where V_0 is the average velocity of the solitons and $d\omega_q/dq$ is the velocity of the magnon itself. Equation (2.13) is very similar in form to Eq. (2.14).

Expression (2.13) is evaluated in Appendix B. Within the condition $2\epsilon J/T \ll 1$, one can use the following approximation:

$$\Delta^c(k) \simeq n_s V_0 [1 + \alpha \sin^2(2k)] ,$$

with $\alpha = \pi/2 - 1 \simeq 0.57$. In Ref. 2, Villain took into account only the velocity V_k of the soliton k: The velocity of the other solitons $V_{k'}$ was ignored. Equation (2.13) will therefore lead to a different result. In particular, the collision rate will never be zero: It will remain at least the contribution $n_s V_0$ given by the collisions induced by the other solitons, because of their own velocity.

As discussed in Appendix B, this broadening effect allows us to relax the condition for energy conservation which occurs explicitly in Eq. (2.11) through the function $\delta(x)$. This function can be replaced by a Lorentzian, the width of which is evaluated (see Appendix B) to be of the order of

$$\omega_q^c(l) \simeq n_s V_0 \{1+0.5\alpha[1-\cos(2q)\cos(2l)]\} \tag{2.15}$$

in the limit $2\epsilon J/T \ll 1$. Equation (2.11) can now be written as

$$S^z(q,\omega)=\frac{S^2}{\pi}\frac{n_s}{4\cos^2(q/2)}\int_0^{2\pi} dl\, p\left[\frac{l+q}{2}\right]\frac{1}{\pi}\frac{\omega_q^c(l)}{[\Omega_q \sin(l)-\omega]^2+\omega_q^c(l)^2}\,. \tag{2.16}$$

For the transverse spin components, we get

$$S^{\perp}(q,\omega)=\frac{1}{2\pi^2}n_s\int_0^{2\pi} dl\cos^2(l/2)p\left[\frac{l+q}{2}\right]\frac{1}{\pi}\frac{\omega_q^c(l)}{[\omega-\Omega_q \sin(l)]^2+\omega_q^c(l)^2}\,. \tag{2.17}$$

In these equations, which will be used for the analysis of our data, there remain no adjustable parameters. A preliminary check of this model can be performed on the data which were presented in Fig. 5 of Ref. 3 as giving the first evidence for soliton fluctuations in $CsCoCl_3$. This is done in Fig. 2. The effects of collisions are at first ignored. The dashed curve displays the square-root divergency of the Villain mode. The dotted-dashed line takes into account the instrumental resolution by a simple convolution of the previous curve with a Gaussian function of width $\Delta_\omega \simeq 0.36$ THz, evaluated from the peak (FWHM) which can be attributed to the incoherent scattering in Fig. 3 of Ref. 3. The solid line is obtained with the same resolution but results from Eq. (2.16), which takes into account the collisions between solitons. The agreement with the data is rather good. The same model will be used in Sec. IV to explain the data for the soliton modes observed at much lower energy and for much smaller values of $q^* = |\pi - q|$.

III. EXPERIMENTAL

A powder of $CsCoCl_3$ was prepared from a 1:1 mixture of CsCl (2N) (Alfa Inorganic) and of $CoCl_3 \cdot 6H_2O$. This

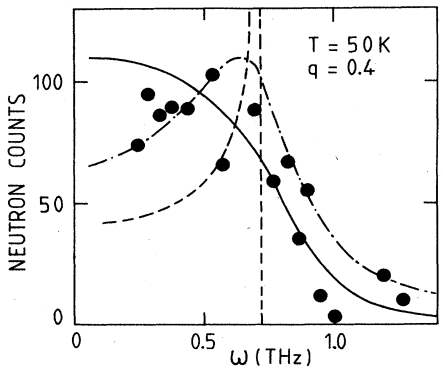

FIG. 2. Neutron data for $CsCoCl_3$ obtained for $S^z(q,\omega)$ at $T=50$ K with $q=0.4$ (rlu) by Yoshizawa *et al.* (Fig. 5 of Ref. 3). The dotted-dashed line shows the prediction of Villain (characterized by a square-root divergency as illustrated by the dashed curve) after an instrumental resolution in energy (FWHM $\Delta_\omega \simeq 0.36$ THz) is taken into account. The solid line displays the effect of collisions between solitons as described by our model [Eq. (2.16)].

mixture was slowly heated to 120 °C under an argon atmosphere and the chlorination was achieved under an anhydrous HCl gas flow. The resulting powder was sealed in a 1.6-cm diameter quartz tube. An Astro carbon furnace heated at 622.0±0.5 °C was used to grow the crystal by a Bridgman method. In the crystallization zone, the gradient of temperature was about 25 °C/cm and the sample, fixed with Mo wires was lowered at a speed of 0.25 cm/h in a graphite tube fitted in a water-cooled pedestal under an upflow of argon of 6 l/min. A very pure single crystal of about 5 cm^3 was thus obtained, a part of which (~ 1 cm^3) was used in our neutron experiments.

The crystal structure of $CsCoCl_3$ is hexagonal with chains of magnetic Co^{2+} ions along the c axis. There are two formula units per unit cell. The structural parameters are $c=5.986$ Å and $a=7.127$ Å (see Fig. 6) at 10 K.[6] The magnetic properties of $CsCoCl_3$ have been widely investigated. Down to the Néel temperature ($T_{N1} \simeq 21$ K), they are quite well described by the 1D Hamiltonian of Eq. (2.1). Below $T_{N1} \simeq 21$ K, specific behavior is expected from the triangular structure in the a-b plane perpendicular to the chains (inset in Fig. 6). As discussed above, a partially disordered phase is observed which can be understood if the coupling between nearest-neighbor chains is antiferromagnetic. Below $T_{N2} \simeq 9$ K, a two-sublattice ferromagnetic structure occurs which can result from the presence of a small second-neighbor ferromagnetic coupling in the a-b plane.[6] A possible intermediate three-sublattice ferrimagnetic phase has also been suggested to develop below 13 K.[6] In the PD phase, one expects one chain out of three to remain disordered, hence in a paramagnetic state. This situation should allow us to observe fluctuations associated with solitons below T_{N1}.

Our neutron inelastic scattering measurements have been carried out using the three-axis spectrometer IN12 situated on a cold-neutron guide tube at the reactor of the Institute Laue-Langevin in Grenoble. Due to the high flux of long-wavelength neutrons, this instrument allows measurements to be made under conditions of very good instrumental resolution. Pyrolytic graphite was used as monochromator and analyzer; a cooled beryllium filter was placed in the incident beam to reduce higher-order contamination. Horizontal collimations after the monochromator, the sample and the analyzer were 30′.

The crystal was mounted in an aluminum can in an atmosphere of helium gas and placed in a cryostat allowing

the temperature to be varied between 2—300 K. The single crystal was oriented with the chain axis in the horizontal plane so that scattering vectors $\mathbf{Q}=(h,h,l)$ could be surveyed. The one-dimensional magnetic correlations give rise to scattering concentrated in (001) planes with l taking only odd values. Therefore to examine the frequency and q widths of the 1D magnetic scattering, frequency and wave-vector scans have been performed around different scattering vectors: $\mathbf{Q}_0=(0.9,0.9,1)$, (1.1,1.1,1), and (1.2,1.2,1) (expressed in rlu).

In order to obtain the scattering cross section $S(\mathbf{Q},\omega)$ an accurate determination of the resolution function of the spectrometer is needed. We have used the same procedure as developed in our study of "broad" solitons in the "classical" chains of the antiferromagnet tetramethylammonium maganese chloride (TMMC) $[(CD_3)_4NMnCl_3]$.[9] In the case of a 1D system, one can use an "effective" one-dimensional resolution function R_{1D} which depends only on the scattering vector $\mathbf{Q}=\mathbf{Q}_0+q\mathbf{C}^*$. The observed intensity can be written as

$$I(\mathbf{Q}_0+q\mathbf{C}^*,\omega)=\int\int R_{1D}(\mathbf{Q}_0,q-q',\omega-\omega') \times S(\mathbf{Q}_0,q',\omega)d\omega' dq' , \quad (3.1)$$

with

$$R_{1D}(\mathbf{Q}_0,q'',\omega'') = A_{1D}(\mathbf{Q}_0)\exp\{-[C_{qq}(q'')^2+C_{\omega\omega}(\omega'')^2+2C_{q\omega}q''\omega'']\} ,$$

and

$$A_{1D}=\frac{1}{\pi}(C_{qq}C_{\omega\omega}-C_{q\omega}^2)^{1/2} .$$

The C_{ij} coefficients $(i,j=q,\omega)$ are related to those of the conventional three-dimensional resolution matrix.[13] The latter have been determined from scans in $(\mathbf{Q},\omega)$ performed through the Bragg peaks (0,0,1), (1,1,1), (1,1,$\bar{1}$), and (1,1,0). In the case of an incoherent scatterer, one has to perform the q integration in Eq. (3.1), and the corresponding energy width (FWHM) is given directly by

$$\Delta_\omega=2[\ln(2/D_{\omega\omega})^{1/2} ,$$

with $D_{\omega\omega}=C_{\omega\omega}-C_{q\omega}^2/C_{qq}$. The values of the C_{ij} coefficients and of the corresponding instrumental resolution widths Δ_ω and $\Delta q=2[\ln(2/C_{qq})]^{1/2}$ as a function of the incident neutron wave vector k_I for the momentum transfer $\mathbf{Q}_0(1,1,1)$ are listed in Table I.

The background I_{BG} and the incoherent nuclear scattering have been measured for the same $\mathbf{Q}$ and the various k_I and fitted by the Gaussian form

$$I(\omega)=I_{BG}+I_0\exp\{-4\ln[2(\omega/\Delta_\omega)^2]\} .$$

For each scan, this contribution has been subtracted from the experimental data. The remaining contribution to be discussed in the following is therefore expected to result only from the magnetic scattering.

For a 1D spin system, the scattering law to be inserted in Eq. (3.1) can be written as

$$S(\mathbf{Q}_0,q,\omega)=B(\mathbf{Q}_0)[(1+\cos^2\beta)S^\perp(q,\omega)+\sin^2\beta S^z(q,\omega)] ,$$

where β is the angle between $\mathbf{Q}_0$ and the c axis. $S^\perp(q,\omega)$ describes the fluctuations perpendicular to the chain axis. The coefficient $B(\mathbf{Q}_0)$ is given by

$$B(\mathbf{Q}_0)=N(e^2\gamma/mc^2)f^2(\mathbf{Q}_0) ,$$

where k_I and k_F are the incident and final wave vectors, respectively, and $f(\mathbf{Q})$ the magnetic form factors of the N Co^{2+} ions involved in the scattering process.

Finally, the experimental intensity defined by Eq. (3.1) can be rewritten as

$$I(\mathbf{Q}_0,q,\omega)=B(\mathbf{Q}_0)[(1+\cos^2\beta)I^\perp(\mathbf{Q}_0,q,\omega) +\sin^2\beta I^z(\mathbf{Q}_0,q,\omega)] , \quad (3.2)$$

with

$$I^{z,\perp}(\mathbf{Q}_0,q,\omega)=\int_{-\infty}^{+\infty}\int_{-\infty}^{+\infty} R_{1D}(\mathbf{Q}_0,q-q',\omega-\omega') \times S^{z,\perp}(q',\omega')dq'd\omega' , \quad (3.3)$$

where $S^{z,\perp}(q,\omega)$ are given by Eqs. (2.7) for the 1D AF mode or (2.16) and (2.17) for the soliton fluctuations.

IV. NEUTRON SCATTERING RESULTS

A. Antiferromagnetic mode: $q\simeq\pi$

Energy and wave-vector scans centered around $\omega=0$ and $q=\pi$ were performed at several temperatures between 13 and 60 K, covering both the 1D paramagnetic and PD phases, for $T>T_{N1}\simeq 21$ K and $T<T_{N1}$, respectively. Some typical energy scans at two temperatures are presented in Fig. 3. The scattering vector was $\mathbf{Q}_0=(1.2,1.2,1)$ or (1.1,1.1,1) in the paramagnetic phase and $\mathbf{Q}_0=(1.1,1.1,1)$ or (0.9,0.9,1) in the PD phase. These latter values have been chosen so as to minimize the con-

TABLE I. Parameters C_{ij} $(i,j=q,\omega)$ of the 1D resolution matrix and instrumental widths $\Delta\omega$ and Δq observed for $\mathbf{Q}_0=(1,1,1)$.

	k_I (Å^{-1}) 1.15	1.55	1.70
C_{qq} (rlu)$^{-2}$	24 000±4000	25 000±4000	30 000±5000
$C_{\omega\omega}$ (THz)$^{-2}$	54 000±5000	18 000±2000	15 000±2000
$C_{q\omega}$ (rlu THz)$^{-1}$	21 000±4000	17 000±3000	20 000±4000
$D_{\omega\omega}$ (THz)$^{-2}$	36 000±4000	7000±600	3000±300
Δ_ω (THz)	0.0090±0.0005	0.020±0.001	0.037±0.002
Δ_q (rlu)	0.011±0.001	0.011±0.001	0.010±0.001

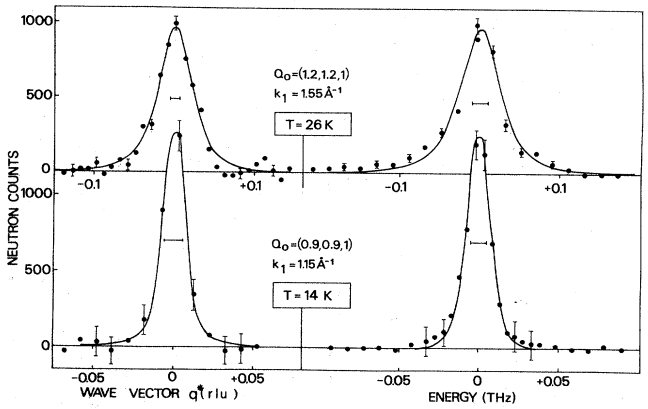

FIG. 3. Central peak in $CsCoCl_3$: typical wave-vector and energy scans performed at $q^*=0$. The solid lines are theoretical curves fitted to the data as described in the text. The horizontal line shows the instrumental resolution.

tribution from the magnetic Bragg peaks which, below T_{N1} occur at $(\frac{2}{3},\frac{2}{3},1)$ and $(\frac{4}{3},\frac{4}{3},1)$ as shown in Fig. 4. At these values of $\mathbf{Q}_0$, the scattering intensity, apart from the small background and incoherent contributions, can be attributed to an underlying magnetic plane associated with chains remaining possibly in a paramagnetic state.

To perform the analysis of data such as shown in Fig. 3, only the scattering law $S^z(q,\omega)$ needs to be considered in Eq. (3.3). A possible contribution from $S^\perp(q,\omega)$ to the observed intensity $I(q,\omega)$ is expected to be negligible. As discussed previously, for $q^*\approx\pi$, the parallel fluctuations result from the flipping of the sublattices in the ordered domains. The number of spins involved in this scattering is given by the average number of spins in the domains. This number is simply the inverse of the soliton density: $n_s^{-1}=\exp(+J/T)$. This number is large ($\gg 1$) at all temperatures and *increases* exponentially as $T\to 0$. On the other hand, the perpendicular fluctuations would be associated only with the spins in the walls, namely the soliton density itself, $n_s=\exp(-J/T)$, which is small ($\ll 1$) and *decreases* exponentially. Therefore, taking into account the instrumental resolutions, we expect any contribution from $S^\perp(q,\omega)$ to be negligible compared to

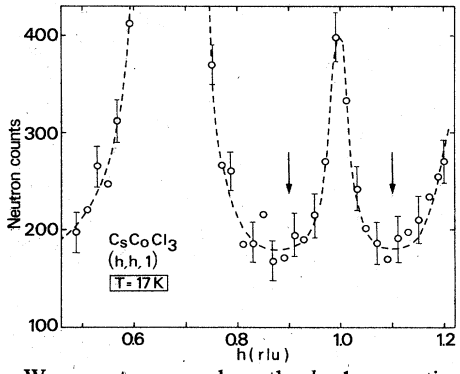

FIG. 4. Wave-vector scan along the $l=1$ magnetic plane for $CsCoCl_3$ at $T=17$ K. The arrows show the positions chosen for the energy scans performed on the magnetic plane below $T_{N1}\simeq 21$ K.

$I^z(q,\omega)$. The curves shown in Fig. 3 are a fit to the data obtained from the simplified expression

$$I(\mathbf{Q}_0,q,\omega)\simeq B(\mathbf{Q}_0)\sin^2\beta I^z(\mathbf{Q}_0,q,\omega)$$

used together with Eqs. (3.3) and (2.7). In the fitting procedure, the widths Γ_q and Γ_ω have been considered as adjustable parameters; the resulting values are plotted in Fig. 5. Also shown are the values obtained previously for Γ_q by Yoshizawa and Hirakawa.[10] In fact, their values have been corrected by a multiplicative factor 1.53/2 [Eqs. (2.8)] in order to account for the characteristic non-Lorentzian shape of $S^z(q,\omega)$ [Eq. (2.7)] (Ref. 9). In Fig. 5 the curves correspond to the theoretical predictions of Sec. II. The solid lines are given by Eqs. (2.2) and (2.6). The dashed line shows the influence of the temperature on Γ_ω at $T\lesssim 2\epsilon J=18$ K by using the exact expression (2.5) for V_0. Since no adjustment of any physical parameters was made, the agreement between the soliton model and the experiments is extremely good over the whole temperature range, i.e., above and *below* $T_{N1}\simeq 21$ K ($1/T_{N1}\simeq 0.048$).

The full scattering intensity which would be obtained after a double integration in both q and ω is performed over $I(\mathbf{Q}_0,q,\omega)$ [Eq. (3.2)]:

$$I(\mathbf{Q}_0)=\int_{-\infty}^{+\infty}\int_{-\infty}^{+\infty} d\omega I(\mathbf{Q}_0,q,\omega)\sim B(\mathbf{Q}_0)\sim N$$

is an interesting quantity to be known as it gives an evaluation of the number N of spins involved in the neutron scattering. In the present case, it can allow us to determine the relative number of chains contributing to the paramagnetic fluctuations observed above and below T_{N1}. When the scattering law is such a smooth decreasing function as given by Eq. (2.7), a straightforward evaluation of $I(\mathbf{Q}_0)$ is given by the product

$$I(\mathbf{Q}_0)\propto I_{\max}\delta_q\delta_\omega\ , \tag{4.1}$$

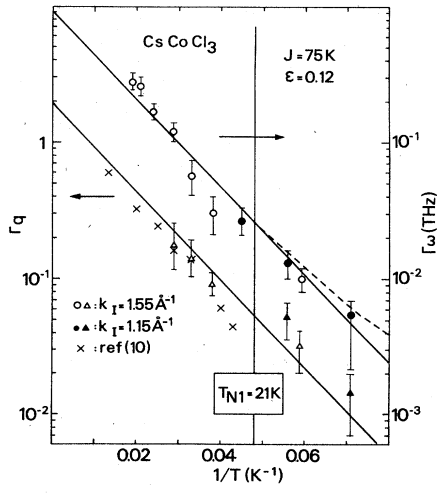

FIG. 5. Experimental values of Γ_q and Γ_ω plotted on logarithmic scales as a function of $1/T$. Γ_q is a number which gives the soliton density according to Eq. (2.2). The crosses are obtained from Ref. 10. The solid lines are the theoretical predictions [Eqs. (2.2) and (2.6)]. The dashed line takes into account the temperature dependence of V_0 [Eq. (2.5)].

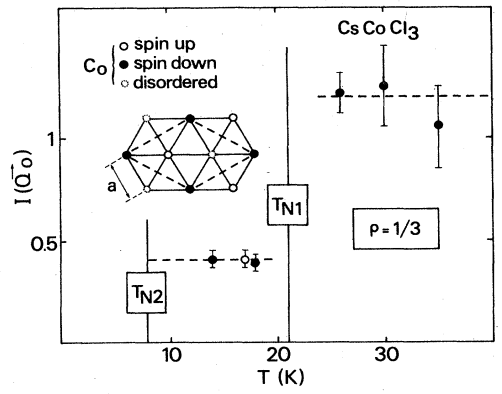

FIG. 6. Intensity "integrated" over q and ω [Eq. (4.1)] of the AF mode as a function of T, above and below $T_{N1}\simeq 21$ K. The inset indicates schematically the frustrated triangular spin structure below T_{N1}.

where $I_{\max}$, δ_q, and δ_ω are, respectively, the experimental maximum intensity, the widths in q and in ω of the mode observed in the measurements. The values obtained for $I(\mathbf{Q}_0)$ at different temperatures are shown in Fig. 6. As expected they are temperature independent but different below and above T_{N1}. The average intensity below T_{N1} is approximately $\frac{1}{3}$ of that above T_{N1}.

This result agrees completely with the relative number of chains expected to remain disordered in the PD phase. From this study of the AF mode we can conclude first that the disorder is *dynamic*. Second, due to the good agreement between the data of Fig. 5 and Eqs. (2.2) and (2.6), we conclude also that the dynamics are governed by moving solitons.

B. Soliton mode: $q^* = |\pi - q| \gg \Gamma_q$

To observe the soliton fluctuations, the value of the associated wave vectors $q^* = |\pi - q|$ must be larger than the inverse of the correlation length $\kappa = \Gamma_q$. Our investigation of the soliton mode has been made with the scattering vector $\mathbf{Q}_0 = (1.1, 1.1, 1 - q^*)$ and with $x = q^*/\Gamma_q \gtrsim 3$. Some data obtained for various values of q^* (or x) and temperatures are shown in Figs. 7 and 8.

First, we notice that the same type of fluctuations are observed over the whole temperature range $13 \lesssim T \lesssim 30$ K, i.e., above and below $T_{N1}\simeq 21$ K. Second, we observe that the inelastic intensity is rather flat up to frequencies close to the theoretical value $\Omega_q = 4\epsilon J \sin q$ (displayed by the dashed vertical lines) after which the intensity starts to decrease smoothly. No maximum is observed despite the high instrumental resolution used in these measurements.

So that we can compare data obtained with different incident wavelengths we have followed the normalization procedure described in detail by Dorner.[14] The essential feature of this procedure is that for data collected at different wavelengths, but with the counting time controlled by a monitor detector, the intensity defined by Eq. (3.2) must be multiplied by factors of the form:

$$k_F^3 \cot\theta_A \ ,$$

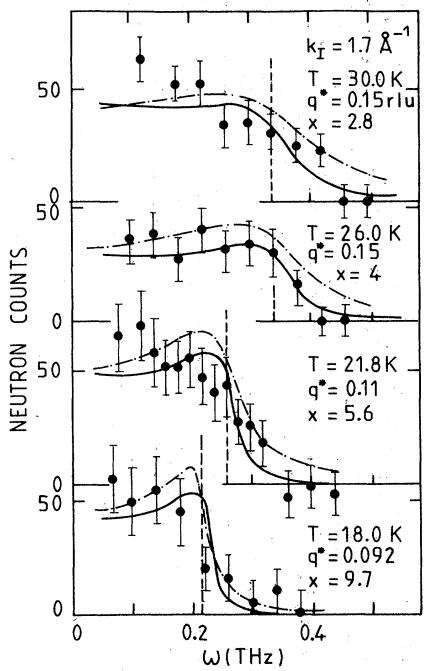

FIG. 7. Energy scans performed at $\mathbf{Q}_0 = (0.0, 0.9, 1 - q^*)$ (rlu) for $k_I = 1.70$ Å^{-1} for different temperatures above and below $T_{N1} = 21$ K. The solid lines are theoretical curves which take into account both the collisions between solitons and the instrumental resolution. The dotted-dashed lines ignore the instrumental resolution. As T decreases, so does the soliton-mode intensity [Eqs. (2.16) and (2.3)]. To observe the soliton mode at lower temperature, it is necessary to move to smaller q^*.

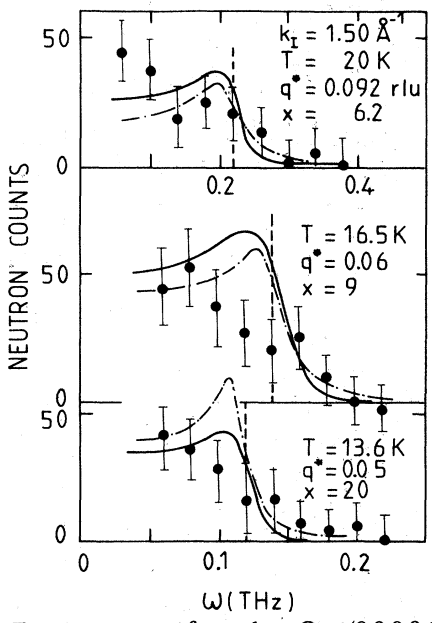

FIG. 8. Energy scans performed at $\mathbf{Q}_0 = (0.9, 0.9, 1 - q^*)$ for $k_I = 1.55$ Å^{-1} for different temperatures below $T_{N1} = 21$ K. The curves are defined as in Fig. 7.

where θ_A is the relevant analyzer angle.

Finally for a quantitative comparison between theory and experiment over the whole temperature range, the intensity of the curves has been adjusted to the data at only one temperature, arbitrarily chosen to be $T=26.0$ K [Fig. 7(b)]. A good agreement is obtained; the intensities, the frequency widths and the shapes are reasonably well reproduced. The dotted-dashed lines shown on the same figures ignore the instrumental resolution and are derived directly from (2.16) and (2.17). They show that for $T > T_{N1} \simeq 21$ K, the absence of peak results more from the damping due to the collisions between solitons rather than from the instrumental resolution.

This good agreement, which we emphasis, is in fact a surprising result. As the temperature is lowered through $T_{N1} \simeq 21$ K, we expect the observed intensity to decrease by a factor of 3 since we know from Sec. IV A that the number of chains remaining uncorrelated is three times smaller below T_{N1}. Since no apparent change is observed experimentally, this suggests that fluctuations associated with solitons persist even in ordered chains. This may be a result of the particular conditions of small q^* and small energy chosen in our experiments. It could mean that soliton excitations maintain relatively rapid motions even in presence of magnetic ordering. This is an important point which should be examined in more detail, experimentally and theoretically, in future work.

V. CONCLUSION

Several important results have been established in this work. One relies on the good agreement between all the experimental data and our "completed" soliton model: the collisions between solitons play an essential role and cannot be ignored in a description of the soliton fluctuations. Another gives an experimental proof that in $CsCoCl_3$, one third of the chains remains uncorrelated below T_{N1} and that the chain dynamics is governed by moving solitons. Finally, it is suggested that fluctuations associated with solitons persist in the ordered chains.

The good agreement mentioned above is obtained when a careful description of the fluctuations is used. From the analysis of the AF mode, we have checked firstly that in such pure crystals, "narrow" solitons in "quantum" chains move coherently as do "broad" solitons in classical chains.[1] This is established by the relation between the q and ω widths of the AF mode ($\Gamma_\omega = V_0 \Gamma_q$) [Eq. (2.4)], which has been verified over the whole temperature range. This means that after they have been created the solitons retain their initial velocity both in amplitude and direction ($\mathbf{x}=\mathbf{v}t$). Despite their narrow width (one lattice unit) the moving walls seem to be no more affected by local defects than are broad solitons. The approximation given by Maki [Eq. (2.7)] is also important. It leads to good quantitative agreement with the soliton model, obtained without adjustment of any physical parameter. Unfortunately, and despite the exceptional instrumental resolution used here, the characteristic shape of the AF mode [Eq. (2.7)] could not be checked experimentally. Within the experimental uncertainties, a simple Lorentzian form would reproduce just as well the observed line shape. Concerning the soliton modes, the semiphenomenological derivation that we propose for describing the effects of collisions between walls is able to answer the puzzling question why no sharp finite-energy peak is observed in this compound. From Eq. (2.15) taken at the value $2l=\pi$ at which the divergency occurs ($\omega \simeq \Omega_q$), i.e.,

$$\omega_q^c(\pi/2) \simeq n_s V_0 \{1+\alpha[1+0.5\cos(2q)]\} ,$$

one sees that the narrowest peak is obtained for $q=\pi/2$, where the soliton dispersion frequency Ω_q [Eq. (2.12)] is the largest. The observation of such a peak, at relatively high energy ($\Omega_{\pi/2} \simeq 0.63$ THz) with a sufficient instrumental resolution will be difficult. On the other hand, for $q \to \pi$ the collision rate is larger (by a factor $1+2\alpha \simeq 1.9$) and the damping of the soliton modes become more pronounced preventing us from observing any peak. Nevertheless the good agreement obtained with the data under so many conditions of temperature and wave vector confirms the realistic feature of our collision model. Finally one obtains a fully self-consistent description for these fluctuations in terms of solitons alone.

In the partially disordered phase soliton fluctuations have also been observed. One third of the chains remain uncorrelated with free solitons moving along them. In the ordered chains, low-frequency fluctuations persist which could be attributed also to solitons, and it is interesting to compare this result with the EPR signal observed previously by Adachi.[7] The PD phase should extend down to a certain temperature T_{N2} below which a complete three-dimensional (3D) ordering is expected. In Ref. 6, the value $T_{N2} \simeq 9.2$ K was given. T_{N2} can be also determined by following the evolution of the intensity of the 1D AF mode as a function of temperature (Fig. 9). When the 3D ordering occurs, the 1D correlations must vanish. T_{N2} is determined from the maximum of the intensity. We find $T_{N2}=8.5\pm0.2$ K in agreement with Yoshizawa and Hirakawa.[10] In this figure, the solid line is a theoretical curve obtained from the soliton model. Again it describes the data well. No departure from the model of freely moving solitons is observed. We would have expected some effects below 13.5 K, in this intermediate phase, as-

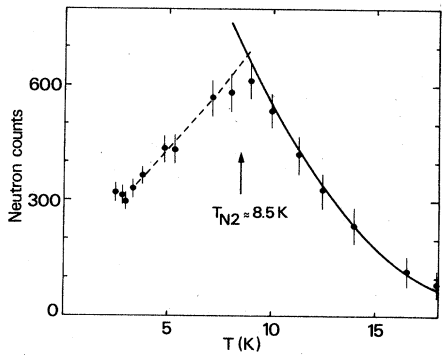

FIG. 9. Temperature dependence of the intensity of the magnetic planes measured at $\mathbf{Q}_0=(0.9,0.9,1)$ below $T_{N1} \simeq 21$ K. The maximum gives an accurate evaluation of the ordering temperature $T_{N2}=8.5\pm0.2$ K. The solid line is a theoretical curve calculated using the soliton model.

sociated with new interchain correlations, as suggested by Yelon *et al.*[6] This would have been consistent with a slowing down of the solitons. Rather, the full ordering seems to occur sharply at T_{N2}, below which a two-sublattice ferrimagnetic structure occurs. The present investigation has shown finally that in such compounds the soliton regime can now be studied over an extremely wide range of temperature, from $T \simeq 75$ K down to 8.5 K.

ACKNOWLEDGMENTS

We are most grateful to F. Devreux, B. Dorner, and J. Villain for useful discussions and to K. Holczer for his help in numerical computations.

APPENDIX A

As in the paper of Villain,[2] the derivation of the soliton fluctuations outlined below is performed in the subspace E_1 of states containing one elementary excitation. For an open chain of N spins such a state is defined as

$$|m+\tfrac{1}{2}\rangle = |+-+-+--+-+-+-\rangle \ .$$
$$1\ 2\ \cdots\ m\ \cdots\ N$$

The first spin of the chain ($n=1$) has been fixed arbitrarily to be $S^z=+\frac{1}{2}$. Hence, at a site n the different spin components S_n^z, $S_n^{\pm}=S_n^x \pm iS_n^y$ are given by

$$\langle m'+\tfrac{1}{2}|S_n^z|m+\tfrac{1}{2}\rangle = (-1)^n \frac{1}{2}\left[\frac{n-m}{|n-m|}\delta_{m\neq n}-\delta_{n,m}\right]\delta_{m,m'} ,$$

$$\langle m'+\tfrac{1}{2}|S_n^{\pm}|m+\tfrac{1}{2}\rangle = \tfrac{1}{2}[1\pm(-1)^n](\delta_{m',m-1}\delta_{n,m}+\delta_{m',m+1}\delta_{n,m+1}) .$$

Defining the spin operators in the reciprocal space of wave vectors q as

$$S_q^{\alpha}=\frac{1}{\sqrt{N}}\sum_{n=1}^{N} S_n^{\alpha} e^{-iqn} ,$$

the corresponding matrix elements are evaluated for an infinite chain to be

$$\langle m'+\tfrac{1}{2}|S_q^z|m+\tfrac{1}{2}\rangle = -\tfrac{1}{2}\frac{\delta_{m,m'}}{\sqrt{N}}\frac{1+e^{-iq}}{2\cos^2(q/2)}e^{-i(q+\pi)m} , \tag{A1}$$

$$\langle m'+\tfrac{1}{2}|S_q^{\pm}|m+\tfrac{1}{2}\rangle = \frac{1}{\sqrt{N}}e^{-iqm}(1\pm e^{i\pi m})\tfrac{1}{2}(\delta_{m',m-1}+e^{-iq}\delta_{m',m+1}) .$$

To obtain Eq. (A1), use has been made of the following relation:

$$\sum_{\lambda=\pm 1}^{\pm\infty} e^{-i(q+\pi)\lambda} = -1/(1+e^{iq}) .$$

In subspace E_1, the eigenvectors of the Hamiltonian $\mathscr{H}$ given by Eq. (2.1) are

$$|k\rangle = \frac{1}{\sqrt{N}}\sum_{m=1}^{N} e^{-ik(m+1/2)}|m+1/2\rangle ,$$

and the matrix elements for the spin operators are obtained to be

$$\langle k'|S_{-q}^z|k\rangle = \frac{1}{2}\frac{i}{\sqrt{N}}\frac{1}{\cos(q/2)}\delta_{k',k-q+\pi} ,$$

$$\langle k'|S_{-q}^{\pm}|k\rangle = \frac{1}{\sqrt{N}}\cos\left[k-\frac{q}{2}\right](\delta_{k',k-q}\pm i\delta_{k',k-q-\pi}) .$$

These expressions are used to calculate directly the correlation functions defined as follows:

$$S^{\alpha}(q,t)=\frac{1}{2\pi}\sum_k n_k\langle k|S_q^{\alpha}(t)[S_q^{\alpha}(0)]^*|k\rangle , \tag{A2}$$

where $n(k)$ is the soliton occupation number for the state $|k\rangle$:

$$n(k)=n_s p(k) , \tag{A3}$$

with the soliton density,

$$n_s=\exp(-J/T) ,$$

and the occupation probability,

$$p(k)=e^{-2\epsilon J\cos(2k/T)}\Big/\sum_k e^{-2\epsilon J\cos(2k/T)} . \tag{A4}$$

Using the operator unity,

$$1=\sum_{k'}|k'\rangle\langle k'| ,$$

and $\mathscr{H}|k\rangle=\omega_k|k\rangle$ with

$$\omega_k=J+2\epsilon J\cos(2k) , \tag{A5}$$

the diagonal elements in Eq. (A2) can be written as

$$\langle k|S_q^{\alpha}(t)[S_q^{\alpha}(0)]^*|k\rangle = \sum_{k'}\langle k|S_q^{\alpha}|k'\rangle\langle k'|(S_q^{\alpha})^*|k\rangle e^{i(\omega_{k'}-\omega_k)t} .$$

Since

$$\omega_{k-q-\pi}-\omega_k=\omega_{k-q}-\omega_k=4\epsilon J\sin q\sin(2k-q) ,$$

one obtains from (A2)

$$S^z(q,t)=\frac{1}{4\pi^2}\frac{n_s}{4\cos^2(q/2)}\int_{-\pi}^{+\pi}dk\,p(k)e^{i4\epsilon Jt\sin q\sin(2k-q)} ,$$

$$S^{\pm}(q,t)=\frac{1}{2\pi^2}n_s\int_{-\pi}^{+\pi}dk\cos^2\left[k-\frac{q}{2}\right]p(k)e^{i4\epsilon Jt\sin q\sin(2k-q)} .$$

The spectral density is obtained by Fourier transforming:

$$S^{\alpha}(q,\omega)=\frac{1}{2\pi}\int_{-\infty}^{+\infty}dt\,e^{-i\omega t}S^{\alpha}(q,t) ,$$

yielding, for instance,

$$S^z(q,\omega)=\frac{1}{4\pi^2}\frac{n_s}{4\cos^2(q/2)}\times\int_0^{2\pi}dl\,p\left[\frac{l+q}{2}\right]\delta[\Omega_q\sin(l)-\omega] , \tag{A6}$$

with $\Omega_q=4\epsilon J\,|\sin q\,|$. After integrating, we obtain for $-\Omega_q\le\omega\le\Omega_q$

$$S^z(q,\omega)=\frac{S^2}{2\pi^2}\frac{2\kappa}{4\cos^2 q/2}\frac{e^{\omega/(2T)}}{I_0(2\epsilon J/T)}\times\frac{\cosh\{\cot[q(\Omega_q^2-\omega)^{1/2}/(2T)]\}}{(\Omega_q^2-\omega^2)^{1/2}}\,,$$

where $I_0(X)$ is the modified Bessel function,

$$I_0(X)=\frac{1}{2\pi}\int_{-\pi}^{+\pi}dk\,e^{-X\cos(2k)}\,, \tag{A7}$$

and for the transverse spin component,

$$S^{\perp}(q,\omega)=\tfrac{1}{2}[S^+(q,\omega)+S^-(q,\omega)]=S^x(q,\omega)=S^y(q,\omega)$$
$$=\frac{1}{(2\pi)^2}\kappa\frac{e^{\omega/2T}}{I_0(2\epsilon J/T)}\left[\frac{\cosh\{\cot[(\Omega_q^2-\omega^2)^{1/2}/(2T)]\}}{(\Omega_q^2-\omega^2)^{1/2}}-\frac{\sinh\{\cot[q(\Omega_q^2-\omega^2)^{1/2}/(2T)]\}}{\Omega_q}\right], \tag{A8}$$

with the inverse correlation length,

$$\kappa=2n_s=2e^{-J/T}\,.$$

In the limit $\epsilon J\ll T\ll J$, we obtain

$$S^z(q,\omega)\simeq\frac{S^2}{2\pi^2}\frac{2\kappa}{4\cos^2(q/2)}\frac{1}{(\Omega_q^2-\omega^2)^{1/2}}\,,$$

and

$$S^{\perp}(q,\omega)\simeq\frac{1}{4\pi^2}\kappa\frac{1}{(\Omega_q^2-\omega^2)^{1/2}}\,.$$

APPENDIX B

As already mentioned in Ref. 2, the collisions between solitons are expected to round off the divergency predicted by the theory described in Appendix A. In the following we try to describe in a semiphenomenological way the effects of such collisions. This procedure can be considered as an extension of what was suggested by Villain.[2]

In the subspace E_1, one expects each energy level associated with the wave vector k to be broadened by the collisions. The characteristic width is given by the collision rate to be

$$\Delta^c(k)\simeq n_s\sum_{k'\,(\neq k)}p(k')\,|\,V_{k'}-V_k\,|\,, \tag{B1}$$

where V_k is the velocity of a soliton in the state k. This quantity is defined Eq. (A5) as

$$V_k=\frac{d\omega_k}{dk}=-4\epsilon J\sin(2k)\,. \tag{B2}$$

In (B1) the sum runs over all k's except the value $k'=k$. However, to within a good approximation it can be extended to all values of k. This leads to the following expression:

$$\Delta^c(k)\simeq n_s\{4\epsilon J\,|\sin(2k)\,|\,[1-I(\eta)/I_0(2\epsilon J/T)]+\frac{4T}{\pi}\sinh[(2\epsilon J/T)\,|\cos(2k)\,|\,]/I_0(2\epsilon J/T)]\}\,, \tag{B3}$$

with

$$I(\eta)=\frac{1}{\pi}\int_{\eta}^{\pi-\eta}dx\,\exp[(-2\epsilon J/T)\cos x\,]\,.$$

The parameter η depends on the range of the k values:

$$0\le k\le\pi/4\rightarrow\eta=2k\,,$$
$$\pi/4\le k\le\pi/2\rightarrow\eta=\pi-2k\,,$$
$$\pi/2\le k\le 3\pi/4\rightarrow\eta=2k-\pi\,,$$
$$3\pi/4\le k\le\pi\rightarrow\eta=2\pi-2k\,.$$

In the limit where the temperature is not small compared to $2\epsilon J$ ($2\epsilon J/T\ll 1$), since $I_0(2\epsilon J/T)\simeq 1$ [Eq. (A7)] and $V_0\simeq 8\epsilon J/\pi$ [Eq. (2.5)], Eq. (B3) becomes

$$\Delta^c(k)\simeq n_s V_0[\eta\,|\sin(2k)\,|+|\cos(2k)\,|\,]\,. \tag{B4}$$

The k dependence of this quantity is displayed in Fig. 10 where it can be seen that Eq. (B4) is well approximated by

$$\Delta^c(k)\simeq n_s V_0[1+\alpha\sin^2(2k)]\,, \tag{B5}$$

with $\alpha=\pi/2-1\simeq 0.57$.

In the calculation of the spectral densities as given by (A6), for instance, one has to consider all the possible transitions between two different states k and k' such that $k'=k-q+\pi$. The broadening of the corresponding energy level as introduced above allows us now to relax the

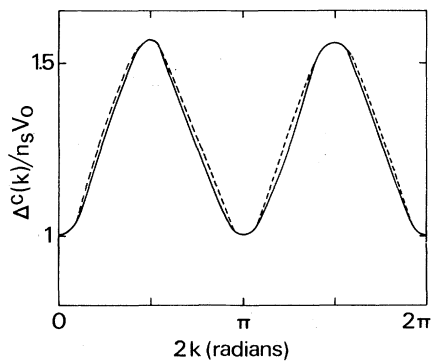

FIG. 10. Rate of collisions between solitons as a function of k defining the plane waves of subspace E_1, as given by Eq. (B4) (solid line). The dashed curve is an approximation corresponding to Eq. (B5).

energy-conservation condition represented by the function $\delta(x)$ in (A6). This function $\delta(x)$ is better replaced by a Lorentzian having a full width of the order of

$$2\omega_q^c(k,k')\simeq\Delta^c(k)+\Delta^c(k') .$$

Using the same parameter $l=2k-q$, as in Eq. (A6), one obtains from (B5),

$$\omega_q^c(l)\simeq n_s V_0\{1+\alpha[1-\cos(2q)\cos(2l)]\} .$$

Equation (A6) now reads

$$S^z(q,\omega)=\frac{1}{4\pi^2}\frac{n_s}{4\cos^2(q/2)}\int_0^{2\pi}dl\,p\left[\frac{l+q}{2}\right]\frac{\omega_q^c(l)}{[\Omega_q\sin(l)-\omega]^2+\omega_q^c(l)^2} ,$$

and Eq. (A8) can now be written as

$$S^{\pm}(q,\omega)=\frac{1}{2\pi^2}n_s\int_0^{2\pi}dl\cos^2(l/2)p\left[\frac{l+q}{2}\right]\frac{\omega_q^c(l)}{[\Omega_q\sin(l)-\omega]^2+\omega_q^c(l)^2} .$$

APPENDIX C

The validity of the previous calculation for $S^z(q,\omega)$ in Appendix A is limited to wave vectors $q\ll|\pi-\kappa|$. For $q\simeq\pi$, we are actually dealing with ordered domains of length $\xi=\kappa^{-1}$. The dynamics results from the motion of the solitons which induces flippings of the magnetic sublattices. The time dependence from the correlation function

$$S^z(z,t)=\langle S_n^z(t)S_{n+z}^z(0)\rangle=S^2\exp[-2N(z,t)]$$

is assumed to decrease exponentially with the number $N(z,t)$ of solitons present at time t in the interval $|z-V_k t|$, where V_k is the soliton velocity given by Eq. (B2). We can write

$$N(z,t)=\frac{1}{N}\sum_{k=-\pi}^{+\pi}|z+4\epsilon Jt\sin 2k|\,n(k) ,$$

with $n(k)$ given by Eq. (A3). Depending on the value of $\eta=|z/4\epsilon Jt|$, two regimes must be considered. For $0\le\eta\le 1$, the solitons may have time to flip the spin at the position $n+z$, thus reducing the correlation which existed initially with the spin at the site n. Defining the average soliton velocity by

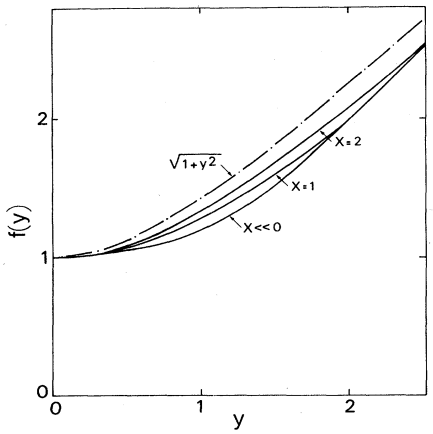

FIG. 11. The function $f(y)$ which is defined by Eq. (C2) is represented for different values of $X=2\epsilon J/T$. The approximation given by Maki (Ref. 8), $f(y)=(1+y^2)^{1/2}$, is also shown.

$$V_0=\frac{1}{N}\sum_{k=-\pi}^{+\pi}|V_k|p(k) , \tag{C1}$$

with the probability $p(k)$ given by Eq. (A4), we get

$$V_0=\frac{2}{\pi}\frac{4\epsilon J}{I_0(2\epsilon J/T)}\frac{\sinh(2\epsilon J/T)}{2\epsilon J/T} ,$$

and, with $X=2\epsilon J/T$:

$$N(z,t)=n_s V_0|t|\left[\frac{X}{\sinh X}\eta\int_0^{\arcsin\eta}dl\cosh(X\cos l)+\frac{\sinh[X\cos(\arcsin\eta)]}{\sinh(X)}\right] .$$

For $\eta\ge 1$, the soliton velocity remains too small to allow any flipping at the site $n+z$ during the time interval t:

$$N(z,t)=n_s|z|=n_s V_0|t|\left|\frac{z}{V_0 t}\right| .$$

The quantity

$$f(y)=N(z,t)/n_s V_0|t| \tag{C2}$$

is plotted as a function of $y=|z/V_0 t|$ in Fig. 11 for different temperatures: $X=2\epsilon J/T\ll 1$, 1, and 2 corresponding to $T\ll 18$, $T\simeq 18$, and $T\simeq 9$ K, respectively, for the case of $CsCoCl_3$. In the same figure the curve for the approximation suggested by Maki[8] is shown also:

$$f(y)=(1+y^2)^{1/2} .$$

This has the advantage of yielding an analytical expression for the spectrum $S^z(q,\omega)$,

$$S^z(q,\omega)=\frac{S^2}{2\pi}\frac{\Gamma_\omega^2/\Gamma_q}{\{\Gamma_\omega^2[1+(q^*)^2/\Gamma_q^2]+\omega^2\}^{3/2}} , \tag{C3}$$

with $\Gamma_q=2n_s$ and $\Gamma_\omega=2n_s V_0$.

Since we have already discussed in a similar problem,[9] Eq. (C3) is an approximation sufficient for analyzing our neutron data. The limitation introduced by the instrumental resolution will prevent us from observing any difference from the exact result which would require a numerical (and rather cumbersome) procedure to calculate $S^z(q,\omega)$.

*Also member of Equipe de Recherche 216 CNRS.

[1]J. P. Boucher, L. P. Regnault, J. Rossat-Mignod, J. P. Renard, J. Bouillot, W. G. Stirling, and F. Mezei, Physica (Utrecht) **120B**, 241 (1983).

[2]J. Villain, Physica (Utrecht) B **79**, 1 (1975).

[3]H. Yoshizawa, K. Hirakawa, S. K. Satija, and G. Shirane, Phys. Rev. B **23**, 2298 (1981).

[4]S. E. Nagler, W. J. L Buyers, R. L. Armstrong, and B. Briat, Phys. Rev. Lett. **49**, 590 (1982).

[5]N. Achiwa, J. Phys. Soc. Jpn. **27**, 561 (1969).

[6]W. B. Yelon, D. E. Cox, and M. Eibschütz, Phys. Rev. B **12**, 5007 (1975); M. Melamud, H. Pinto, J. Makovsky, and H. Shaked, Phys. Status Solidi **63**, 699 (1974); M. Mekata, J. Phys. Soc. Jpn. **42**, 76 (1977); M. Mekata and K. Adachi, *ibid.* **44**, 806 (1978).

[7]K. Adachi, J. Phys. Soc. Jpn. **50**, 3904 (1981).

[8]K. Maki, Phys. Rev. B **24**, 335 (1981).

[9]L. P. Regnault, J. P. Boucher, J. Rossat-Mignod, J. P. Renard, J. Bouillot, and W. G. Stirling, J. Phys. C **15**, 1261 (1982).

[10]H. Yoshizawa and K. Hirakawa, J. Phys. Soc. Jpn. **46**, 448 (1979); K. Hirakawa and H. Yoshizawa, *ibid.* **46**, 455 (1979).

[11]S. E. Nagler, W. J. L. Buyers, R. L. Armstrong, and B. Briat, Phys. Rev. B **28**, 3873 (1983).

[12]E. Allroth and H. J. Mikeska, Z. Phys. B **43**, 209 (1981).

[13]M. J. Cooper and R. Nathan, Acta Crystallogr. **23**, 357 (1967).

[14]B. Dorner, Acta Crystallogr. Sect. A **28**, 319 (1972).